JOINT INSTITUTE FOR AERONAUTICS AND ACOUSTICS

National Aeronautics and Space Administration

Ames Research Center

JIAA TR - 93

Stanford University

CONTROL OF SEPARATED FLOW PAST A CYLINDER USING TANGENTIAL WALL JET BLOWING

BY

Sejong Oh and Leonard Roberts

Stanford University
Department of Aeronautics and Astronautics
Stanford, CA 94305

JULY 1989

This research has been supported by NASA Grant NCC 2-55

Abstract

A theoretical analysis is conducted to study the effect of a tangential wall jet on the control of two dimensional separated flow past a circular cylinder. For a tangential wall jet, the mathematical model derived previously [1,2] is used and the vortex cloud method is adopted for the calculation of the external flow field. For certain limiting cases, the governing equations are simplified and closed forms of solutions for the wall jet parameters can be obtained.

It is observed that the wall jet is very efficient in reducing drag by delaying the separation point in the range of small blowing strength. The suction force induced by the wall jet is negligible compared to the drag due to the external stream. However this suction force increases the drag when the blowing strength is large.

Contents

Nomenclature

b	half width of the wall jet
c	radius of cylinder
C_f	friction coefficient
C_μ	jet blowing coefficient
d	horizontal distance of separation point
G	shape function
K	constant determined experimentally
k	constant determined from the velocity profile
m	number of bound vorticity panels
N	$= kn$
n	constant determined from the velocity profile
p	pressure
q	nondimensional variable for jet flow field
R	radius of curvature of body
s, y	surface coordinate system
t	nondimensional variable for jet flow field, time coordinate
U	free stream velocity
u	tangential component of velocity
v	normal component of velocity
Γ	vortex strength

δ^*	length scale of excess mass
ϵ	eddy viscosity
θ	length scale of excess momentum
ρ	density
σ	complex coordinate
ς	vortex core radius
τ	viscous stress
ϕ	velocity potential
Ψ	stream function
Ω	vorticity distribution
ω	bound vorticity intensity
$< >$	time averaged quantity

Subscripts

0	zero pressure gradient
e	external stream
j	jet
w	wall
m	jet maximum velocity

1. Introduction

The wall jet may be used for the control of circulation around an airfoil. Here its use is investigated for drag reduction by delaying the flow separation in the presence of an adverse pressure gradient. Previous studies[3,4,5] of the wall jet have not provided satisfactory results regarding the relationship between the blowing strength and the amount of drag reduction due to delayed separation.

Recently a simple method[1] has been derived for the two dimensional turbulent wall jet for an incompressible flow, including the effects of the external stream. In this study the wall jet model is applied to the case of the flow around a circular cylinder, which can be easily transformed to other body shapes. The external stream which is imposed on the jet model is calculated using the vortex cloud method.[6,7,8] As a preliminary study for the wall jet application, only the mean quantities averaged for a long time are calculated. Typically attention is focused on the effects of the wall jet strength on the variation of drag force and the displacement of the separation point.

2. Mathematical Model

The mathematical model for a 2 dimensional incompressible turbulent wall jet was derived in Ref. 1 and 2. In this section the model for the wall jet is briefly reviewed and the governing equations for the wall jet are modified for the limiting case of jet boundary conditions. The vortex cloud method is employed to calculate the external flow field. Due to the inviscid nature of the vortex cloud method appropriate assumptions are introduced for the calculation of surface pressure distribution.

2.1 Tangential Wall Jet

2.1.1 Mean Velocity Profiles

The mean velocity profile of the wall jet is approximated as comprising two parts; (1) an inner flow adjacent to the curved surface having the characteristics of a turbulent boundary layer, (2) an outer flow which merges with the external stream and is typical of a free turbulent jet. These profiles are shown in Fig. 1. These two parts can be written as follows

$$u = u_m \left[2 \left(\frac{y}{y_m} \right)^{\frac{1}{n}} - \left(\frac{y}{y_m} \right)^{\frac{2}{n}} \right] \qquad \text{for } y \leq y_m \tag{2.1.1}$$

$$u - u_e = (u_m - u_e) \operatorname{sech}^2 k \left[\frac{y - y_m}{b - y_m} \right] \qquad \text{for } y > y_m \tag{2.1.2}$$

where n depends on the Reynolds number of the jet, and lies in the range 5 to 9. The definition of b, half width of the jet, determines the constant k as

$$k = \tanh^{-1} \frac{1}{\sqrt{2}} = 0.8814 \tag{2.1.3}$$

The location of the maximum velocity y_m can be found by matching the second derivative of the velocity profiles in the two regions. This results in

$$\frac{y_m}{b} = \left[1 + kn\left(1 - \frac{u_e}{u_m}\right)^{\frac{1}{2}}\right]^{-1} \tag{2.1.4}$$

In this study it is assumed that the external velocity u_e is smaller than the jet maximum velocity u_m throughout the jet flow field.

2.1.2 Governing Equations for the Wall Jet

With the assumptions that

(a) the contribution to the overall momentum balance of the shear stress at the wall is small

(b) the effects of the wall curvature are small except where it influences the gradients of pressure and shear stress,

the equations of continuity and momentum for a 2-D incompressible flow are

$$\frac{\partial u}{\partial s} + \frac{\partial v}{\partial y} = 0 \tag{2.1.5}$$

$$u\frac{\partial u}{\partial s} + v\frac{\partial v}{\partial y} = -\frac{\partial}{\partial s}\left(\frac{p}{\rho}\right) + \frac{\partial}{\partial y}\left(\frac{\tau}{\rho}\right) \tag{2.1.6}$$

where the pressure and the shear stress are determined from

$$\frac{\partial}{\partial y}\left(\frac{p}{\rho}\right) = \frac{u^2}{R+y} \tag{2.1.7a}$$

$$\frac{\tau}{\rho} = \epsilon\left(\frac{\partial u}{\partial y} - \frac{u}{R}\right) \tag{2.1.7b}$$

where R is the radius of curvature of the body surface and ϵ is an eddy viscosity.

The equation obtained by combining Eqs. (2.1.5) and (2.1.6) can be written in integral form as

$$\frac{d}{ds}\left(\theta\, u_e^2\right) + \frac{du_e}{ds}\left(\delta^*\, u_e\right) = -\frac{\tau_w}{\rho} \tag{2.1.8}$$

where θ and δ^* are the excess of the momentum and mass thicknesses in the wall jet respectively, and are defined as follows:

$$\theta = \int_0^\infty \frac{u}{u_e}\left(\frac{u}{u_e} - 1\right) dy \tag{2.1.9a}$$

$$\delta^* = \int_0^\infty \left(\frac{u}{u_e} - 1\right) dy \tag{2.1.9b}$$

Substitution of the velocity profiles given in Eqs. (2.1.1) and (2.1.2), ignoring higher order terms and the small shear stress at the wall results in

$$\frac{d}{ds}\left[b(u_m - u_e)\left(u_m + \frac{2}{5}u_e\right)\right] + \left[\frac{3}{4}b(k+1)(u_m - u_e)\right]\frac{du_e}{ds} = 0 \tag{2.1.10}$$

Another equation can be obtained from the momentum equation at $y = y_m$, with an appropriate eddy viscosity model, as

$$\frac{1}{K}\frac{d}{ds}\left(u_m^2 - u_e^2\right) + \frac{(u_m - u_e)^2}{b}\left(1 - \frac{y_m}{b}\right)^{-1} + \frac{n}{k}\frac{(u_m - u_e)^{\frac{3}{2}}\, u_m^{\frac{1}{2}}}{R} = 0 \tag{2.1.11}$$

where K is a constant to be determined experimentally.

These two equations, (2.1.10) and (2.1.11) are the governing equation for the two jet parameters b and u_m.

2.1.3 Curvature-Induced Suction at the Wall

Even though the wall jet reduces drag by delaying separation, it causes a rearward suction force due to attachment of the jet to the surface before separation - the

Coanda effect. This amount of suction force can be calculated by integrating the radial momentum equation given by Eq. (2.1.7a) as

$$p_s - p_e = -\int_0^\infty \frac{u^2 - {u_e}^2}{R+y} dy \tag{2.1.12}$$

where s represents the value at the wall surface.

With the definition of θ and δ^* it can be reduced to the approximate result

$$p_s - p_e = -\frac{(\theta + \delta^*) u_e^2}{R + \frac{b}{2}} \tag{2.1.13}$$

2.1.4 Wall Jet Separation

For a turbulent boundary layer the separation condition[1] may be written as

$$\frac{\theta \frac{d}{ds}\left(\frac{p}{\rho}\right)}{\tau_{w,0}} = 5 \tag{2.1.14}$$

Using the definition of θ and the velocity profiles given in Eqs. (2.1.1) and (2.1.2), this condition for the wall jet with large n can be written as follows

$$\frac{1}{K}\frac{d}{ds}\left(\frac{p}{\rho}\right)_e = \frac{5}{2}\frac{u_m^2}{b}\frac{C_f}{K}\left[1 + kn\left(1 - \frac{u_e}{u_m}\right)^{-\frac{1}{2}}\right] + \frac{1}{K}\frac{d}{ds}\left[\frac{(\theta + \delta^*) u_e^2}{R + \frac{b}{2}}\right] \tag{2.1.15}$$

where C_f is defined as

$$C_f = \frac{\tau_w}{\frac{1}{2}\rho {u_m}^2} \tag{2.1.16}$$

2.1.5 Dimensionless Forms of the Equations

The following nondimensional variables are used

$$q = \frac{b(u_m - u_e) u_m}{c\, u_\infty^2}, \quad t = \frac{u_e}{u_m}, \quad \overline{u} = \frac{u_e}{u_\infty} \tag{2.1.17}$$

where c is cylinder radius and $\overline{u}$ is known a priori from the external flow field.

In the case of a cylinder the radius of curvature $R = c$. With these variables and normalizing all the length scales with the cylinder radius c, Eqs. (2.1.10) and (2.1.11) become

$$\frac{d}{ds}\left[q\left(1+\frac{2}{5}t\right)\right]+\left[\frac{3}{4}(k+1)\,qt\right]\frac{1}{\overline{u}}\frac{d\overline{u}}{ds}=0 \tag{2.1.18}$$

$$\frac{1}{K}\frac{d}{ds}\left[\frac{\overline{u}^2\left(1-t^2\right)}{t^2}\right]+\frac{(1-t)^3}{qt^4}\overline{u}^4\left[\frac{1+kn(1-t)^{\frac{1}{2}}}{kn\,(1-t)^{\frac{1}{2}}}\right]+\frac{n}{k}\frac{(1-t)^{\frac{3}{2}}}{t^2}\overline{u}^2=0 \tag{2.1.19}$$

From now on and in the equations shown above, even though all the symbols representing the length scale are quantities normalized with c, the same symbols are used for convenience.

These two equations, (2.1.18) and (2.1.19), are solved subjected to the conditions

$$q|_{s=0}=\frac{b(0)\left(u_j-u_e(0)\right)u_j}{u_\infty^2} \tag{2.1.20a}$$

$$t|_{s=0}=\frac{u_e(0)}{u_j} \tag{2.1.20b}$$

where u_j is the velocity at the jet slot.

When $b(0)$ becomes 0, the ideal case of a jet slot, u_j becomes infinite to maintain a finite momentum injection and these boundary conditions reduce to

$$q(0)\simeq\frac{b(0)u_j^2}{u_\infty^2}=C_\mu \tag{2.1.21a}$$

$$t(0)=\frac{u_e(0)}{u_j}\simeq 0 \tag{2.1.21b}$$

Rearranging Eqs. (2.1.18) and (2.1.19), the following set of ordinary differential equations can be obtained

$$\frac{dt}{ds}=\frac{t}{2\overline{u}^2}\left(1-t^2\right)+\frac{K}{2}\frac{\left(1-t^2\right)^3\overline{u}^2}{qt}\frac{1+N(1-t)^{\frac{1}{2}}}{N(1-t)^{\frac{1}{2}}}+\frac{tKN}{2k^2}(1-t)^{\frac{3}{2}} \tag{2.1.22}$$

$$\frac{dq}{ds} = -\frac{qt}{5\overline{u}^2}\frac{\left(1-t^2\right)}{1+0.4t}\frac{d\overline{u}^2}{ds} - \frac{K}{5}\frac{(1-t)^3\,\overline{u}^2}{(1+0.4t)}\frac{1+N\,(1-t)^{\frac{1}{2}}}{Nt\,(1-t)^{\frac{1}{2}}}$$

$$-\frac{qtKN}{5k^2}\frac{(1-t)^{\frac{3}{2}}}{1+0.4t} - \frac{3(k+1)}{8}\frac{qt}{1+0.4t}\frac{1}{\overline{u}^2}\frac{d\overline{u}^2}{ds} \tag{2.1.23}$$

where $N = kn$

These two equations are solved simultaneously using the 4^{th} order Runge-Kutta method.

Eq. (2.1.13) for the pressure at the wall can be written in terms of q and t

$$\frac{p_s - p_e}{\frac{1}{2}\rho {u_\infty}^2} = -\frac{4}{3k}q\left[\frac{1+\left(\frac{2}{5}+\frac{3}{4}(k+1)\right)t}{1+\frac{1}{2}\frac{t^2q}{\overline{u}^2(1-t)}}\right] \tag{2.1.24}$$

and the separation condition given by Eq. (2.1.15) is

$$\begin{aligned}\frac{1}{K}\frac{1}{\frac{1}{2}\rho {u_\infty}^2}\left(\frac{dp}{ds}\right)_e =& \frac{5}{2k}\left(\frac{kC_f}{K}\right)\frac{\overline{u}^4(1-t)}{t^4q}\left[1+kn\,(1-t)^{\frac{1}{2}}\right] \\ &+\frac{1}{K}\frac{4}{3k}\frac{d}{ds}\left[\frac{q\left(1+\left(\frac{2}{5}+\frac{3}{4}(k+1)\right)t\right)}{1+\frac{1}{2}\frac{t^2q}{\overline{u}(1-t)}}\right]\end{aligned} \tag{2.1.25}$$

2.1.6 Reduced Equation around the Singular Point

The above two equations (2.1.22) and (2.1.23) show a singular behavior around the jet exit where the boundary conditions given by Eqs. (2.1.21a,b) are imposed. To avoid this singularity, the two equations can be expressed around the region of small t as

$$\frac{dq}{ds} \simeq -\frac{K}{5}\frac{1+N}{N}\frac{\overline{u}^2}{t} \tag{2.1.26}$$

$$\frac{dt}{ds} \simeq \frac{K}{2}\frac{1+N}{N}\frac{\overline{u}^2}{qt} \tag{2.1.27}$$

Combining theses two equations with the condition given by Eq. (2.1.21) the closed form solutions for q and t can be obtained as

$$q = C_\mu \exp(-0.4t) \tag{2.1.28}$$

and

$$t = \overline{u}\sqrt{K\frac{1+N}{N}\frac{s}{C_\mu}} \tag{2.1.29}$$

These solutions are applied to the region around the jet exit.

Eq. (2.1.29) shows that t increases rapidly, which means that u_m decreases quickly. This indicates that in the vicinity of the slot, the escaped jet diffuses rapidly. This phenomena causes a sudden increase of b, as can be seen in Eq. (2.1.28).

2.2 Calculation of the External Flow Field

In this study, it is assumed that the wall jet affects the external flow field by changing the separation position and, thereby, the external pressure distribution. Thus for an assumed separation point the external flow field can be calculated separately from the jet flow field. The external flow field is calculated using the vortex cloud method, such that at each time step a new vortex is generated from the separation point.

2.2.1 Vortex Cloud Method

It is well known that the vortex cloud method is very efficient for the calculation of a two dimensional unsteady separated flow field.

For a 2-D flow field, the governing equation and the boundary conditions, in terms of the stream function Ψ, can be written as[6]

$$\nabla^2 \Psi = -\Omega \tag{2.2.1}$$

$$\Psi = \text{const.} \qquad \text{on surface} \tag{2.2.2a}$$

$$\Psi = U\ \Im\sigma \qquad \text{in the far field} \tag{2.2.2b}$$

where $\Im$ represents the imaginary part of a complex value and Ω is the vorticity distribution in the flow field which is replaced by a cloud of vortices of finite core size to avoid infinite induced velocities.

Introducing the core radius ς and the vortex strength Γ_i for the i^{th} vortex, Ω can be written as

$$\Omega(\sigma, t) = \sum_{i=1}^{N} \frac{\Gamma_i}{\varsigma^2} G\left(\frac{|\sigma - \sigma_i|}{\varsigma}\right) \tag{2.2.3}$$

where G is a shape function common to all vortices.

In this study the core radius ς is kept constant throughout the calculation procedure.

The shape function and the associated velocity distribution used in this study were derived by Spalart[8]

$$\pi G = \begin{cases} 0 & \varrho \geq 1 \\ 3(\varrho^2 - 1)^2 & \varrho \leq 1 \end{cases} \tag{2.2.4}$$

$$\frac{2\pi v \varsigma}{\Gamma_i} = \begin{cases} \frac{1}{\varrho} & \varrho \geq 1 \\ \varrho(3 - 3\varrho^2 + \varrho^4) & \varrho \leq 1 \end{cases} \tag{2.2.5}$$

where $\varrho = |\sigma - \sigma_i| / \varsigma$.

A new discrete vortex is generated from the prescribed separation point at each time step such that the flow field including the new vortex satisfies an appropriate

Kutta condition at the separation point. In an unsteady flow field the vorticity is continuously supplied to the surrounding fluid from a separation point such that the strength and the position of the shed vorticity allow for pressure continuity to exist. In this study a simple Kutta condition[6] is used to reduce computational cost. Using this technique the new vortex position and strength are determined as

$$\Gamma_{\text{new}} = 2{u_s}^2 \Delta t \tag{2.2.6}$$

$$\sigma_{\text{new}} = \sigma_s + \mathbf{e}_s u_s \Delta t \tag{2.2.7}$$

where s represent the quantity at the separation point and $\mathbf{e}_s$ is the tangential unit vector at the separation point. Δt is the time increment of the calculation procedure

2.2.2 Numerical Implementation

The cylinder surface is represented by vorticity panels of linearly varying strength. If the surface is divided into m vorticity panels and there are n vortices in the separated flow field, as shown in Fig. 2, the stream function at the control point i is

$$\begin{aligned} \Psi_i = & \oint \omega(\sigma_j) K(\sigma_i, \sigma_j) d\sigma_j \\ & + \frac{1}{2\pi} \sum_{k=1}^{n} \Gamma_k \log|\sigma_i - \sigma_k| + U \Im \sigma_i \end{aligned} \tag{2.2.8}$$

where $\omega(\sigma_j)$ is the bound vorticity density at the j^{th} panel and $K(\sigma_i, \sigma_j)$ are the geometric influence coefficients, which depend only on body geometry.

The first term on the right-hand side of Eq. (2.2.8) is the contribution of the bound vorticity panels, and the second is the contribution of the discrete vortices representing the separated flow field. The last term is due to the free-stream.

Boundary condition (2.2.2a) gives

$$\Psi_1 = \Psi_2 = \cdots = \Psi_m = \text{const.} = c \tag{2.2.9}$$

Conservation of vorticity requires

$$\oint \omega_j d\sigma_j + \sum_{k=1}^{n} \Gamma_k = 0 \tag{2.2.10}$$

There are $m+1$ unknowns; m ω's and c, the value of the stream function at the wing trace. Eqs. (2.2.8), (2.2.9) and (2.2.10) constitute a linear system of $m+1$ equations.

The calculation procedure by solving the equations (2.2.8), (2.2.9) and (2.2.10) is repeated for a time period large enough to obtain mean flow field quantities. At each time step a new vortex is generated from the prescribed separation point and convected with the velocity induced by the neighboring vortices and the bound vorticity panel.

For computational efficiency the following techniques are used to reduce the number of vortices in the flow field and to avoid numerical singularities.

(1) if the vortices come closer to each other than a given value the two vortices are allowed to merge into one and the position and strength are determined such that linear and angular momentum before and after merging are conserved.

(2) if the vortices approach closer to the surface than a given value the vortices are made to disappear

(3) if the velocity induced on the surface by the vortices located far downstream is less than a given value the vortices are made to disappear

2.2.3 Calculation of Mean Pressure and Velocity

From the unsteady Bernoulli equation, the pressure coefficient can be written as

$$C_p = 1 - \left(\frac{u_e}{U}\right)^2 - \frac{2}{U^2}\frac{\partial \phi}{\partial t} \tag{2.2.11}$$

The velocity at the surface can be obtained from the definition of bound vorticity intensity as[7]

$$\frac{u_e}{U} = \frac{\omega}{U} \tag{2.2.12}$$

The mean quantities are obtained as follows

$$< C_p >= \frac{1}{T}\int_0^T C_p dt \tag{2.2.12a}$$

$$< u >= \frac{1}{T}\int_0^T \frac{u}{U_\infty} dt \tag{2.2.12b}$$

where T is the total time during the calculation proceeded.

2.3 Overall Calculation Procedure

Once the mean quantities of the external stream are obtained from the vortex cloud method, these values are substituted into equations (2.1.22) and (2.1.23) to calculate the jet parameters q, t and C_μ, which satisfy the separation condition (2.1.25) at the prescribed separation point. Since the boundary condition (2.1.21) causes a singularity at the jet exit, the approximated solutions (2.1.28) and (2.1.29) for q and t are applied to the first bound vorticity panel from the jet exit. The parameters, q and t, are calculated from the jet exit to the separation point.

Drag can be calculated by integration of the surface pressure, which can be obtained from Eqs. (2.1.24) and (2.2.11). The vortex cloud method provides a realistic pressure distribution when the vortices are located far from the surface.[6] For the present problem, however, the separated vortices stay close to the surface

in the aft-separation region, where the viscous effect are also significant.[9] Here the pressure is assumed constant after separation, an assumption that is adopted in many studies for the cylinder problem.

3 Results and Discussion

In this study it is assumed that the wall jet affects the external flow field by changing the separation point. Although this assumption is valid only for a small blowing strength less than 0.05,[10] the blowing strength is allowed to vary to larger values to investigate the quantitative trends of the flow quantities. The value of n, the parameter for the mean velocity profile, is taken as 7 and C_f, the friction coefficient, is chosen as 0.01. The overall flow pattern and jet slot position are shown in Fig. 3.

3.1 Results

Fig. 4 shows the wake patterns behind a cylinder for four different separation positions. From the figure, it can be seen that the wake width reduces, while the frequency increases as the separation point is delayed. In the case of $d/c = 0.26$, (which is the natural separation observed experimentally without jet blowing) the separation angle is 106 deg. and only three vorticity clusters exist in the given downstream region, but for $d/c = 0.8$ four of those exist. The variation in width of the wake is also clearly visible from the figures.

Fig. 5 shows the amount of suction force due to the wall jet, given by Eq. (2.1.24). The pressure difference across the jet is very small. The blowing strength for this case is very large, its value is almost 1, since for small values of blowing strength the pressure difference can be barely observed.

Fig. 6 shows the variation of pressure distribution on the cylinder surface for

different separation points. As the separation point is delayed, the pressure distribution is recovered to that of the potential calculation without separation except for the small amount induced by the wall jet.

Fig. 7 shows the velocity distribution in the wake at a downstream location. One is for the case of natural separation, $d/c = 0.26$, and the other is for $d/c = 0.7$. This figure clearly shows the difference in the momentum deficit of the wake, which causes a drag on the cylinder. The momentum deficit is reduced significantly with a delay of the separation position.

Fig. 8 shows the variation of jet parameters for different blowing strengths. The limit solutions given as Eqs. (2.1.28) and (2.1.29) are applied only to the first panels after the jet exit and the full equations, (2.1.22) and (2.1.23), are applied to the rest of the region. Fig. 8a shows the variation of t, the ratio of external velocity to jet maximum velocity. t increases rapidly close to the jet exit, indicating a sudden decrease of the jet maximum velocity due to diffusion of the jet. The diffusion in the jet also can be seen in Fig. 8b. Fig. 8a also shows that far from the jet slot the maximum velocity relative to the external velocity reduces with a constant rate regardless of blowing strength, while q varies with a different slope for different blowing strengths as can be seen in Fig. 8b.

Fig. 9 shows the variation of drag coefficient with blowing strength. In the region of small blowing strength, a slight change of C_μ causes a significant decrement of drag. For instance when $C_\mu = 0.06$, which corresponds to $d/c \simeq 0.6$, the drag is reduced to almost 1/3 of that without blowing. This phenomena shows the very efficient mechanism of wall jet blowing with a small amount of momentum injection. For large blowing strength, the drag does not change much with further increments of C_μ. As can be seen in the figure, drag even increases with C_μ, due to the suction

force induced by the jet. Also in this region the assumption that the jet does not affect the external flow field could be violated.

Fig. 10 shows the amount of separation delay with respect to C_μ. This figure shows trends similar to the variation of C_D. Small increments of C_μ provide large separation delays in the small C_μ region. For the large C_μ region, even with a large variation of C_μ, the separation point does not change appreciably.

3.2 Concluding Remarks

An analytical study of a tangential wall jet applied to the control of separated flow past a cylinder has been conducted. The external flow field has been calculated using the vortex cloud method and a mathematical model for a 2-D incompressible turbulent wall jet was applied inside the wall jet flow field.

The vortex cloud method provides a good prediction of the external flow quantities, such as surface velocity distribution and wake pattern. As the separation point is delayed, the width of the wake is reduced and the frequency of the Karman-vortex-street increases.

It is observed that the thin tangential wall jet is very efficient in drag reduction by delaying separation for small blowing strengths, but is not efficient for large blowing strength. For large blowing strength drag even increases due to suction of the jet.

Although this study provides a reasonable indication of the relation between C_μ and C_D, it is desirable to have experimental data to validate the analysis. In this study only mean quantities of the external stream are imposed on the jet model to separate the calculation process between the external stream and the jet flow field.

The wall jet model is limited by the assumption $u_m > u_e$ throughout the jet flow field. Whereas experiments[4,11] have shown that u_e may exceed u_m due to severe adverse pressure gradients around the blunt trailing edge. The assumption, $u_m > u_e$, can be eliminated, however, by the introduction of a additional parameter in the mean velocity profile as in Ref. 3.

This study also assumes that the jet does not affect the external flow field except by changing the separation point. This assumption is valid for small blowing strength; for large blowing strength, the external flow could be influenced by the jet as suggested in Fig. 11.[11]

References

1 L. Roberts, JIAA TR in preparation

2 L. Roberts, "A Theory for Turbulent Curved Wall Jets ", AIAA Paper 87-0004, 1987

3 J. Dunham, "A Theory of Circulation Control by Slot-Blowing, Applied to a Circular Cylinder ", *J. Fluid Mech.*, Vol. 33, pp495-514, 1968

4 S. H. Goradia and G. T. Colwell, "Parametric Study of a Two-Dimensional Turbulent Wall Jet in a Moving Stream with Arbitrary Pressure Gradient ", *AIAA Journal*, Vol. 9, pp 2156-2165, 1971

5 I. S. Gartshore and B. G. Newman, "The Turbulent Wall Jet in an Arbitrary Pressure Gradient ", Aeronautical Quartly, Vol. 20, pp. 25-56

6 S. Oh and D. Tavella, "Application of the Vortex Cloud Method to Slender, Flapped Delta Wings ", AIAA Paper 88-2561, 1988

7 C. S. Lee and S. Bodapati, "Calculation of the Unsteady Flow Field of an Airfoil with a deflected Spoiler by Vortex Cloud Method ", JIAA TR-62, 1985

8 P. R. Spalart and A. Leonard, "Computation of Separation Flows by a Vortex Tracing Algorithm ", AIAA Paper 81-1246, 1981

9 J. H. Gerrad, "The Mechanism of the Formation Region of Vortices behind Bluff Bodies ", *J. Fluid Mech.*, Vol. 25, pp. 401-413, 1966

10 K. T. Lee, "Controlled Vortical Flow on Delta Wings through Unsteady Leading Edge Blowing ", Ph. D. Thesis, Stanford University, 1989

11 H. Irwin, "Measurements in a Self-Preserving Plane Wall Jet in a Positive

Pressure Gradient ", *J. Fluid Mech.*, Vol. 61, pp. 33-, 1973

12 N. J. Wood, "The Aerodynamics of Circulation Control Airfoils ", JIAA TR-41, 1981

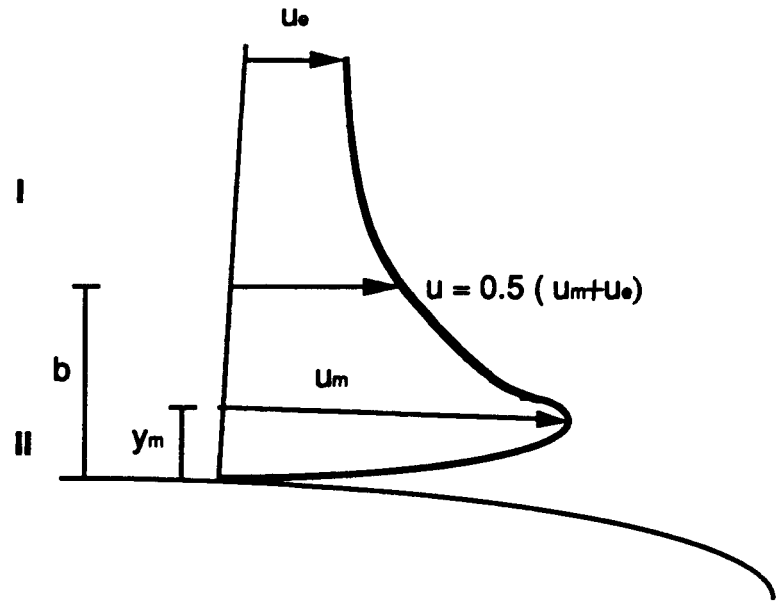

Fig. 1 Velocity profile around jet flow field

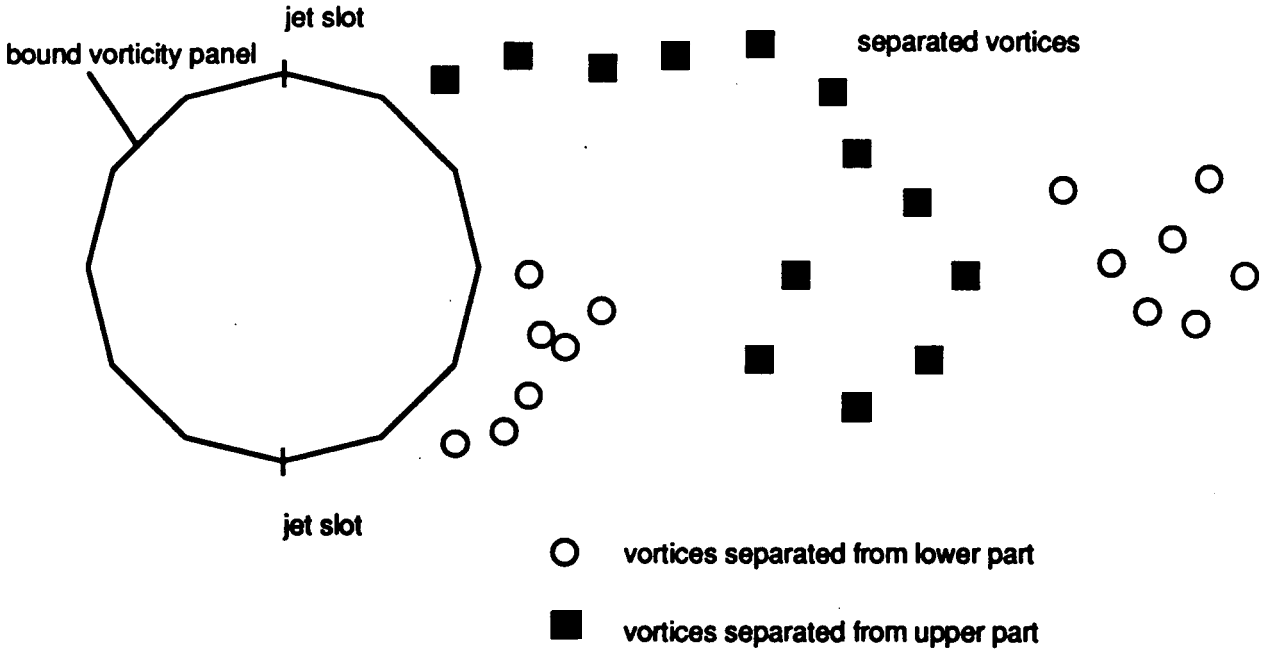

Fig. 2 Bound vorticity panels and separated vortices

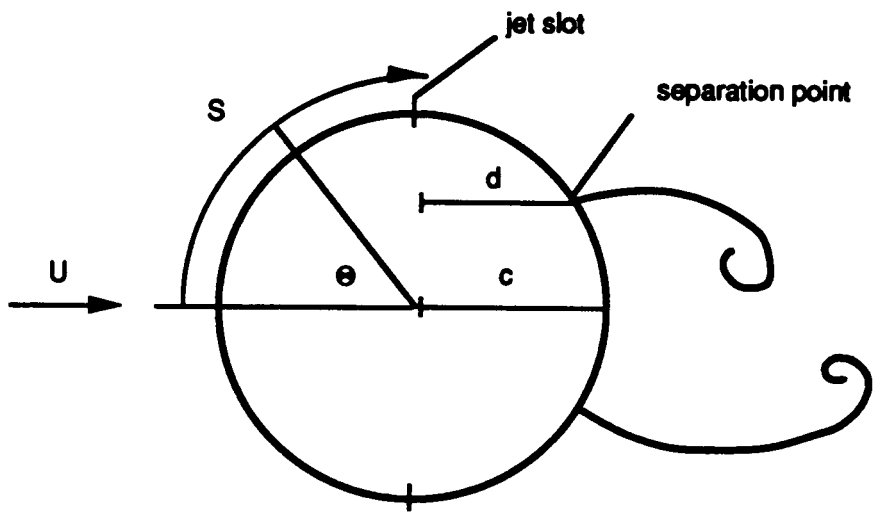

Fig. 3 Overall flow field configuration

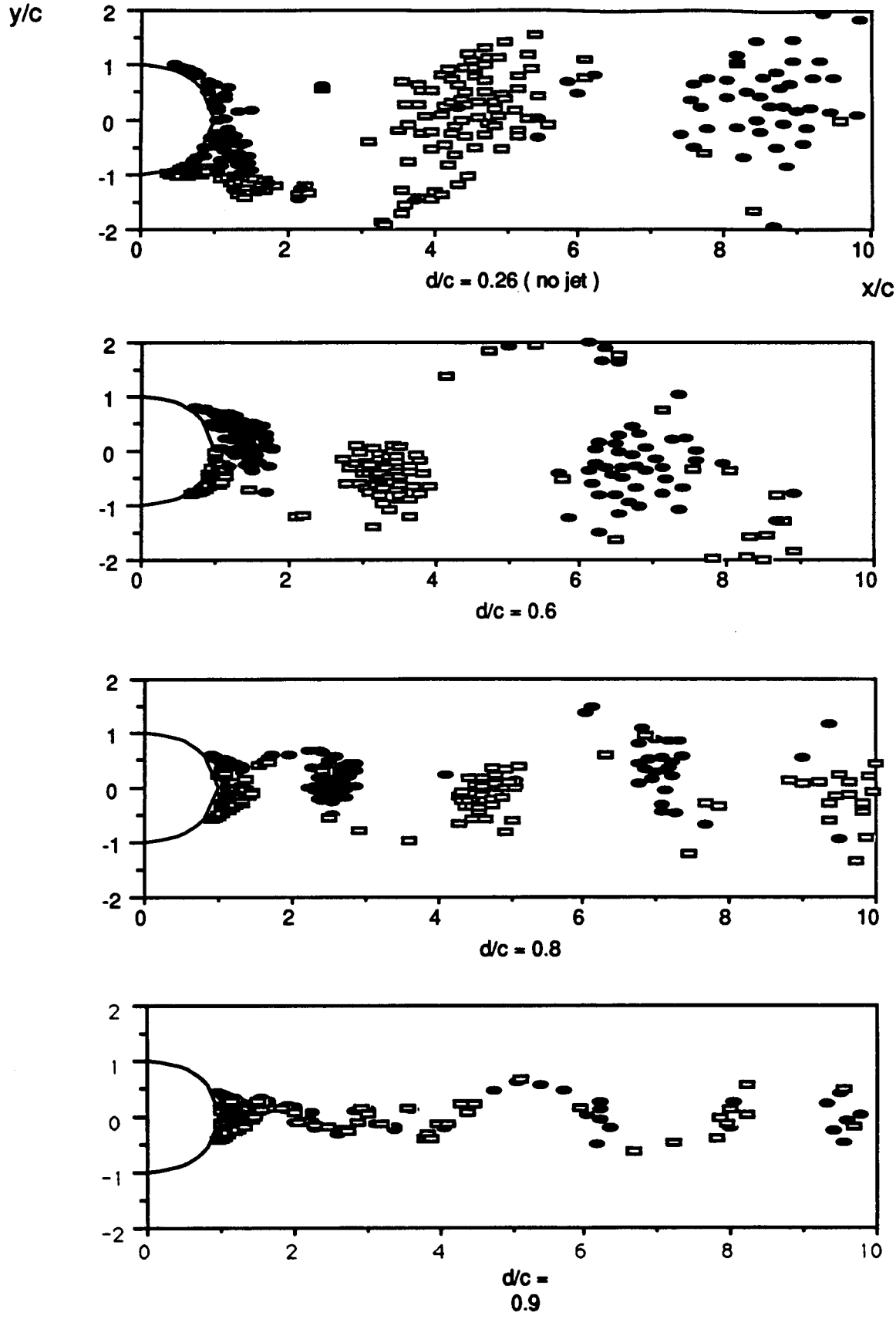

Fig. 4 Wake patterns for different separation points

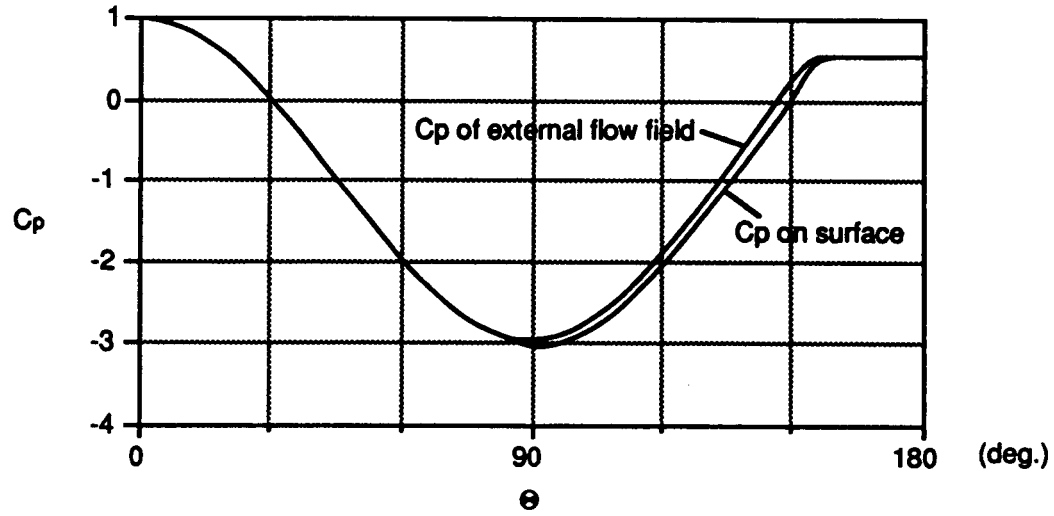

Fig. 5 Effect of jet on wall pressure

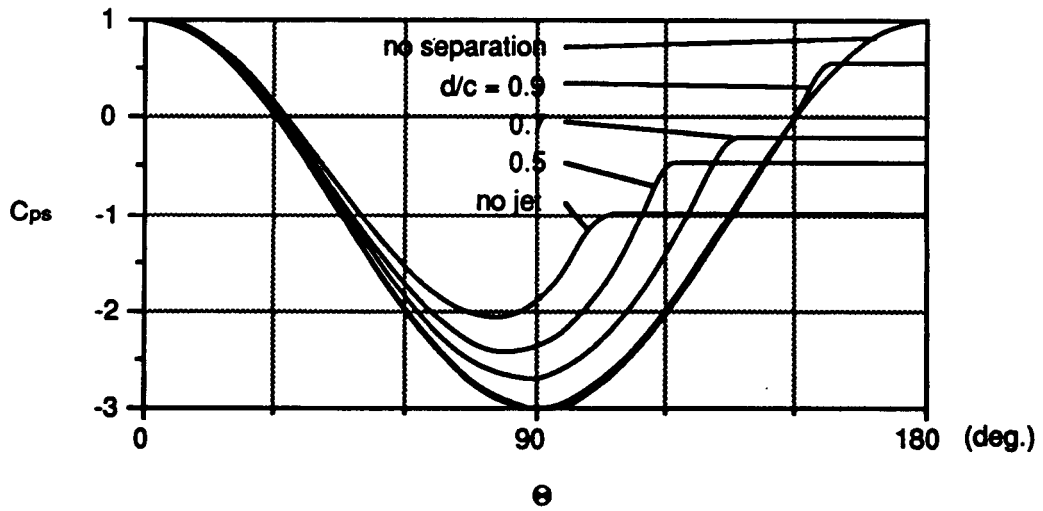

Fig. 6 Pressure distribution for different separation points

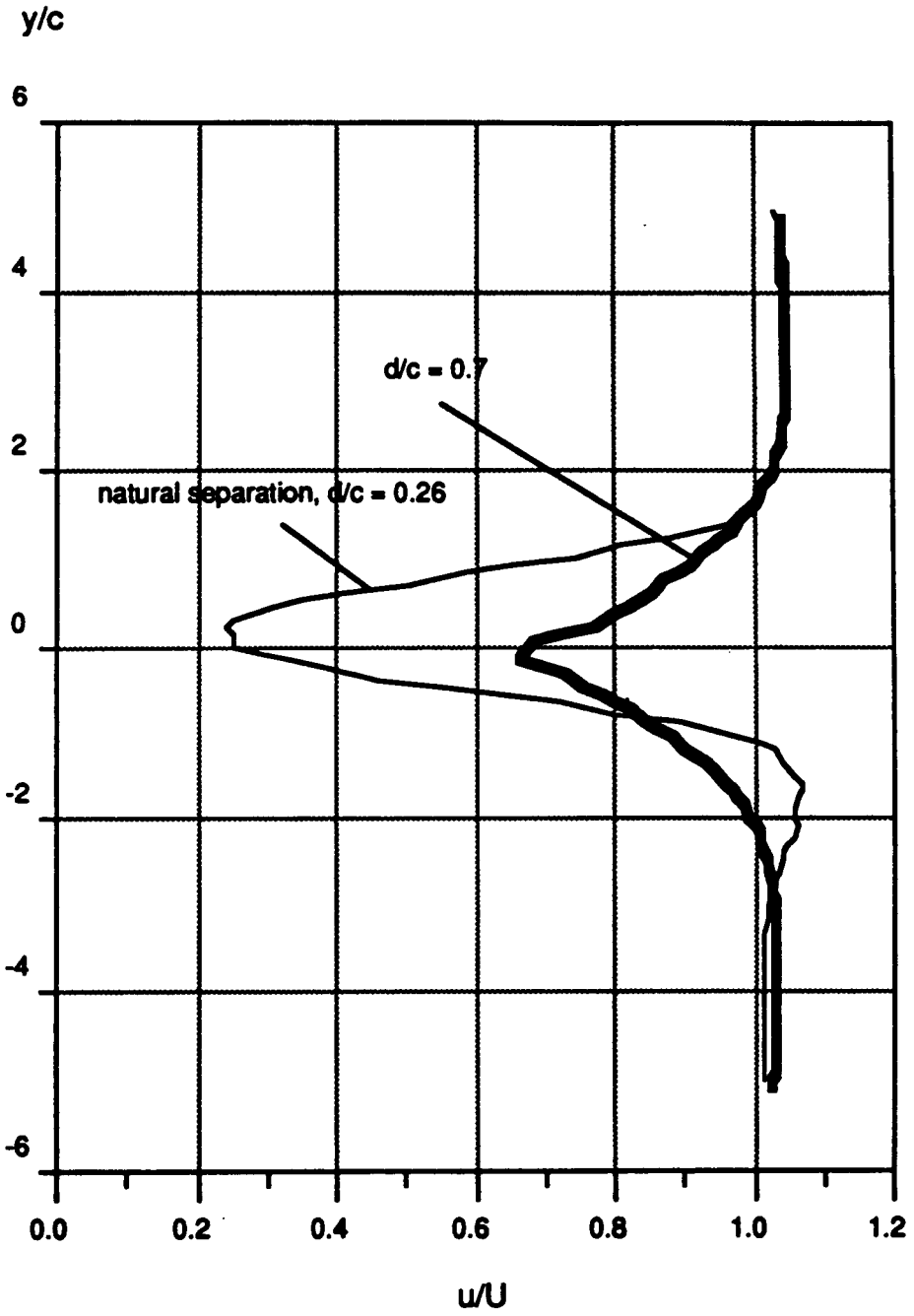

Fig. 7 Momentum deficit at x/c = 2 for two different separation points

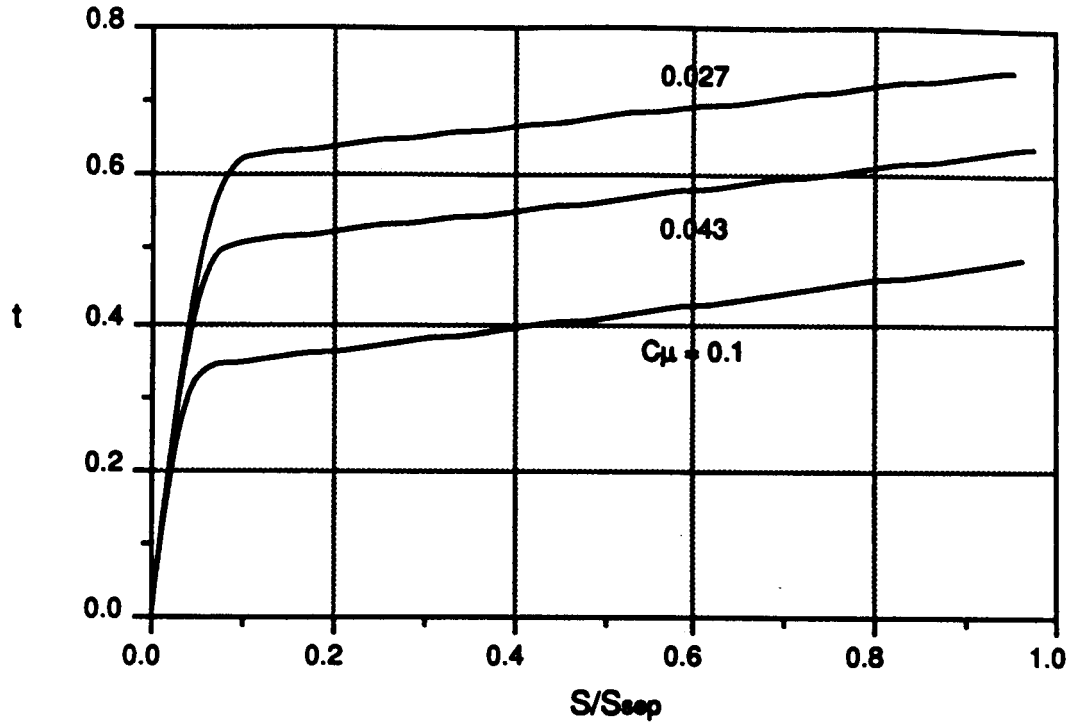

Fig. 8 a Variation of t from the jet slot to the separation point

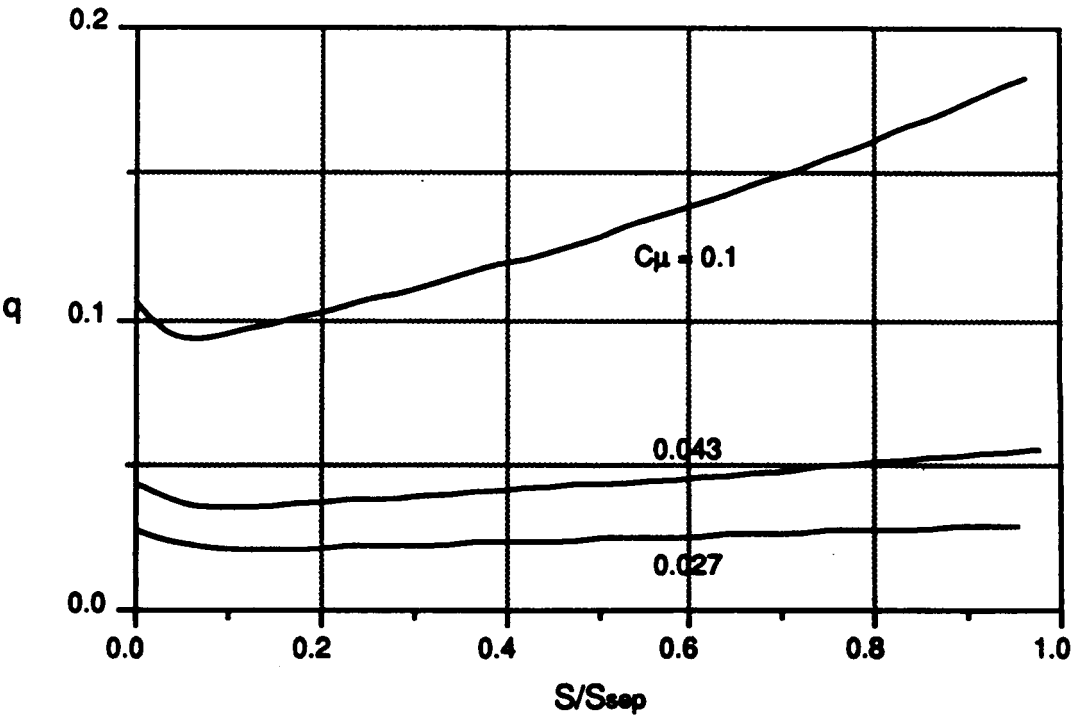

Fig. 8 b Variation of q from the jet slot to the separation point

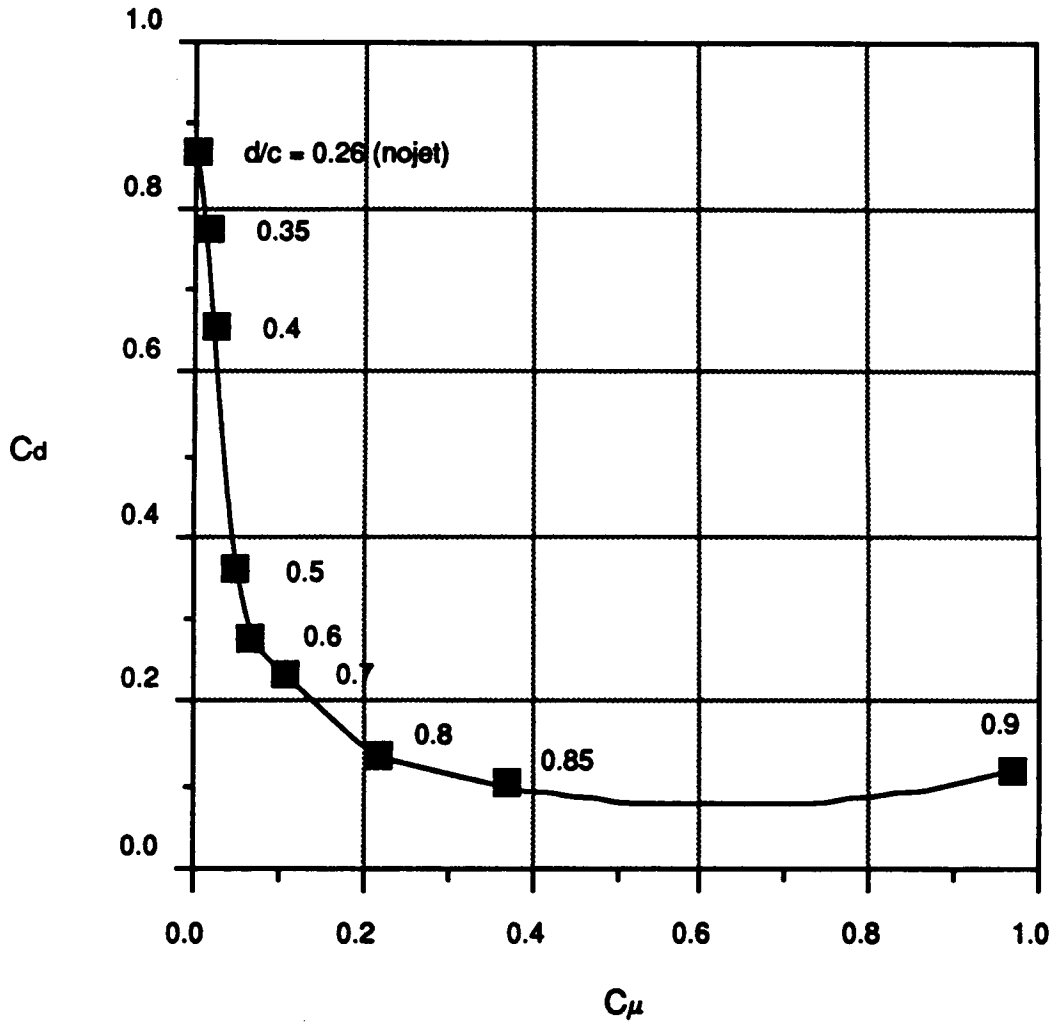

Fig. 9 Variation of drag coefficient with blowing strength

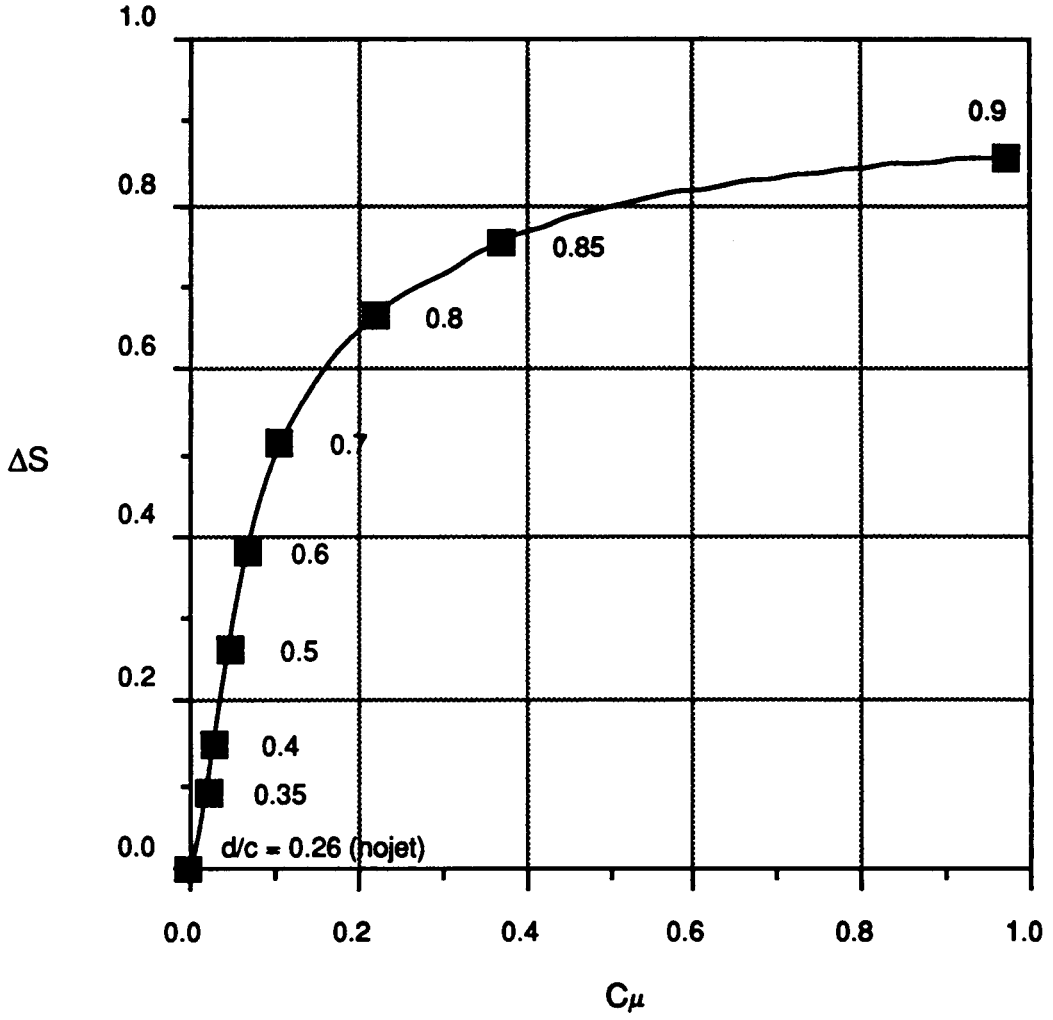

Fig. 10 Amount of separation delay with blowing strength

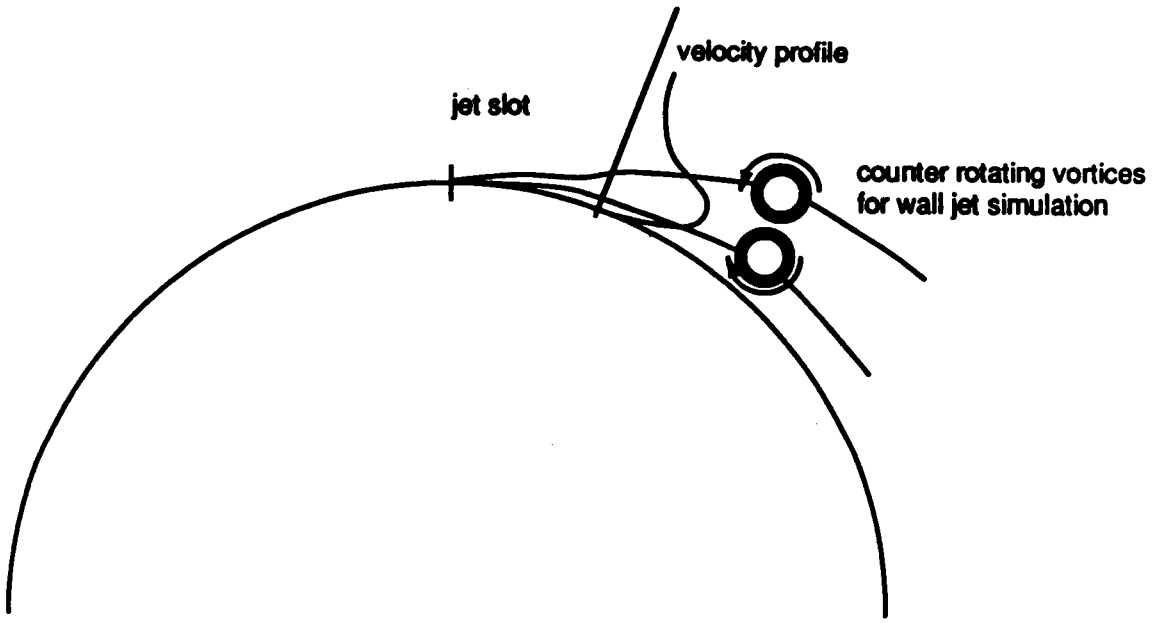

Fig. 11 Vorticity shedding patterns for large blowing strength